Field-free switching of perpendicular magnetization
by cooperation of planar Hall and orbital Hall effects

Zelalem Abebe Bekele[1,2], Yuan-Yuan Jiang[3,4], Kun Lei[1,2], Xiukai Lan[1], Xiangyu Liu[1,2], Hui Wen[1,2], Ding-Fu Shao[3,*], and Kaiyou Wang[1,2,*]

[1] *State Key Laboratory for Superlattices and Microstructures, Institute of Semiconductors,*

Chinese Academy of Sciences, Beijing 100083, China

[2] *Center of Materials Science and Optoelectronics Engineering,*

University of Chinese Academy of Sciences, Beijing 100049, China

[3] *Key Laboratory of Materials Physics, Institute of Solid State Physics, HFIPS,*

Chinese Academy of Sciences, Hefei 230031, China

[4] *University of Science and Technology of China, Hefei 230026, China*

[*]Email: dfshao@issp.ac.cn, kywang@semi.ac.cn

Spin-orbit torques (SOTs) generated through the conventional spin Hall effect and/or Rashba-Edelstein effect are promising for manipulating magnetization. However, this approach typically exhibits non-deterministic and inefficient behaviour when it comes to switching perpendicular ferromagnets. This limitation posed a challenge for write-in operations in high-density magnetic memory devices. Here, we determine an effective solution to overcome this challenge by simultaneously leveraging both a planar Hall effect (PHE) and an orbital Hall effect (OHE). Using a representative Co/PtGd/Mo trilayer SOT device, we demonstrate that the PHE of Co is enhanced by the interfacial coupling of Co/PtGd, giving rise to a finite out-of-plane damping-like torque within the Co layer. Simultaneously, the OHE in Mo layer induces a strong out-of-plane orbital current, significantly amplifying the in-plane damping-like torque through orbital-to-spin conversion. While either the PHE or OHE alone proves insufficient for reversing the perpendicular magnetization of Co, their collaborative action enables high-efficiency field-free deterministic switching. Our work provides a straightforward strategy to realize high-speed and low-power spintronics.

Spintronics employs spontaneous magnetic states in materials for encoding information in nonvolatile memories, logic devices, and neuromorphic computing[1,2]. A high-performance spintronic device requires the efficient manipulation and detection of magnetic states, which is crucial for write-in and read-out operations. The ferromagnets with perpendicular magnetizations are desirable for high-density applications. So far, the efficient electric manipulations of perpendicular ferromagnets remain a challenging problem. A promising approach is the spin-orbit torque (SOT), where an in-plane charge current J (x direction) generates a nonequilibrium spin polarization p, which exerts a damping-like torque $\tau \sim m \times (m \times p)$ on the magnetization m of a ferromagnetic layer (FM) in a SOT device[3-6]. In the conventional spin Hall effect (SHE)[3,4] or the Rashba-Edelstein effect (REE)[5,6] that is widely used in the SOT devices, the generated p is usually aligned to the direction of $J \times z$, i.e. the p_y, due to the symmetry constraint, where z is a direction normal to the film plane. However, the switching by the associated in-plane damping-like torque $\tau_y \sim m \times (m \times p_y)$ is inefficient and non-deterministic. First, a large current is required to generate a sufficiently strong p_y and the associated τ_y, since τ_y need to overcome the precession induced by the anisotropy field. Second, the τ_y can only pull m toward y direction while applying the current, and the relaxation of m cannot be controlled when the current is released[7]. Experimentally, an external assisting magnetic field along the x direction (H_x) is usually required to assist the switching by τ_y[3-7], which eventually generates additional energy consumption harmful to low-power applications. The need for H_x can be eliminated by an exchange bias field or a stray field induced by an adjacent magnetic layer[8-11], the device structure engineering[12,13,14], or the localized laser annealing[15]. Recently, a straightforward solution has been proposed to introduce an additional z-spin component in p (p_z), as the generated out-of-plane damping-like torque $\tau_z \sim m \times (m \times p_z)$ can directly reverse the m without the assisting H_x magnetic field[16,17,18]. Moreover, when p_z is sufficiently strong, the switching current can be significantly reduced since the associated τ_z does not compete with magnetic anisotropy but directly changes the effective damping in ferromagnets[17,18]. Extensive efforts have been made to generate the p_z in SOT devices, such as using a spin source with low crystal symmetry[19,20,21] and/or an additional magnetic order[19-26], the competing spin currents[27-30] or the interface engineering via combined actions of spin-orbit filtering, spin precession, and scattering[31-34].

Despite these advancements, generating a strong p_z for τ_z-dominated switching in SOT devices remains quite challenging. However, it is possible to design a straightforward strategy for an efficient

τ_y-dominated SOT switching. This can be achieved by leveraging the collaborative action of moderate p_z and a significantly enhanced p_y. The moderate p_z enables field-free functionality acting similar to an assisted external field, while the enhanced p_y effectively reduces the switching current necessary for switching. This approach holds the potential to offer a scalable solution for the practical implementation of field-free SOT devices, characterized by low power consumption. Here, we present an effective method for achieving field-free switching of perpendicular magnetization by combining a planar Hall effect (PHE) and an orbital Hall effect (OHE). The former enables the generation of a finite p_z within the perpendicular ferromagnet itself, while the latter produces a transverse orbital current, capable of being converted into a *y*-polarized spin current with greater strength than that generated by conventional SHE and REE. We show that in a Co/PtGd/Mo heterostructure, the PHE in the Co layer is significantly enhanced by interfacing with a PtGd layer, resulting in a moderate p_z. Simultaneously, the Mo layer contributes a strong OHE, amplifying p_y generation through efficient orbital-to-spin conversion. While these effects individually prove insufficient for reversing the perpendicular magnetization of Co, their synergistic cooperation efficiently realizes deterministic switching without the need for an external magnetic field.

The PHE is a transport phenomenon in magnetic materials where a longitudinal current J_x generates a transverse current $J_\perp$ when $\boldsymbol{m}$ is lying within the J_x-$J_\perp$ plane. It arises from the intrinsic anisotropic magnetoresistance (AMR) in the ferromagnets and the generated $J_\perp$ is spin-polarized along $\boldsymbol{m}$. Therefore, PHE can generate an out-of-plane spin current carrying p_z in a perpendicular ferromagnet[35], eliminating the requirement of special spin sources or low symmetric interfaces in conventional mechanisms for p_z generation. This p_z maybe employed in a conventional SOT device to assist the switching by p_y. However, this approach has not been demonstrated yet, possibly due to that PHE in common ferromagnetic metals is not sufficient to assist the switching by SHE or REE with an achievable current density. To realize this approach in practice, one needs to find a strategy to efficiently enhance PHE for a moderate p_z, and use a new mechanism beyond SHE or REE to boost p_y. We propose the PHE can be enhanced by engineering the interfacial exchange coupling between the perpendicular ferromagnet layer and a suitable adjacent layer, and the sufficiently large p_y can be generated by including an additional layer in the SOT device to generate OHE.

We begin by highlighting the enhancement of PHE in the SOT devices illustrated in Fig. 1a-1c. A 0.8 nm ferromagnetic Co layer was deposited atop the commonly employed spin source Pt layer

with a thickness of 2 nm (denoted as Co(0.8)/Pt(2), as shown in Fig. 1a). The good perpendicular magnetic anisotropy (PMA) of the Co layer is confirmed by the measurement of AHE resistance (R_H), as shown in Fig. 1d. Since PHE is proportional to AMR, we measure the longitudinal resistance of this device under a magnetic field rotating within the x-y and x-z plane. We find the AMR is relatively small in Co(0.8)/Pt(2), since AMR originates from spin-orbit coupling (SOC), which is small for Co even interfaced with the heavy metal Pt. Considering that the AMR may be enhanced in the presence of a stronger interfacial coupling, we replace the Pt layer with a PtGd alloy layer with the stoichiometry of $Pt_{0.65}Gd_{0.35}$. Gd is an element with a significant effective magnetic moment and strong SOC. Although the magnetic order in PtGd alloy is absent[28], a thin Pt-Gd-Co alloy intermediate layer may appear across the interface between the Co and PtGd layer, which may be ferromagnetic and strongly coupled with the top Co layer[36], and thus may introduce substantial enhancement of AMR in Co layer. This is clearly shown in Fig. 1d-1f, where the AMR for Co(0.8)/PtGd(2) sample is much stronger than that of Co(0.8)/Pt(2). We notice that the AMR can be further enhanced in the presence of a Mo layer underneath the PtGd, which may be due to the introduction of electrons carrying orbital angular momentum that can enhance the anisotropic scattering.
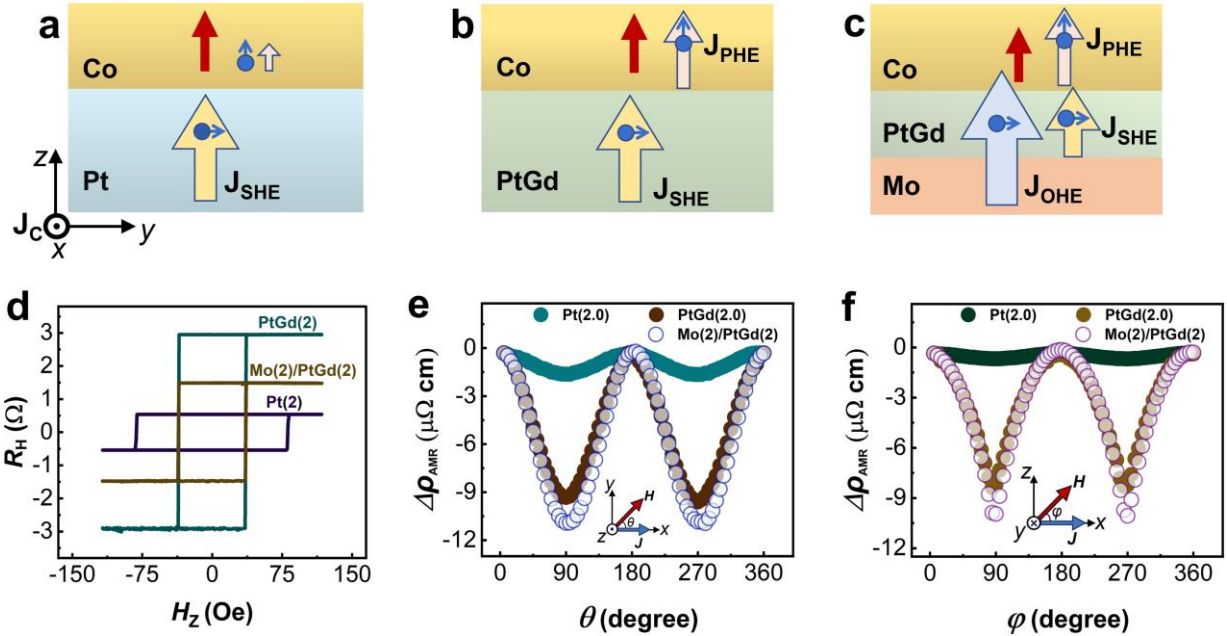

Figure 1: **Schematic of Co/PtGd/Mo SOT devices and their basic magneto-transport properties.**

(**a**) A Co/Pt bilayer SOT device. The Co layer has perpendicular anisotropy. A current J along the x direction generates a negligible out-of-plane z-polarized spin current by PHE (J_{PHE}) in

Co layer and a moderate out-of-plane y-polarized spin current by SHE (J_{SHE}) in Pt layer. The J_{SHE} enters Co layer and exerts a moderate τ_y. (**b**) A Co/PtGd bilayer SOT device where PtGd supports a moderate J_{SHE}, and the J_{PHE} in Co layer is enhanced due to the Co/PtGd interface coupling. The J_{PHE} can exert an additional τ_z in Co layer besides τ_y due to J_{SHE}. (**c**) A Co/PtGd/Mo trilayer SOT device. In addition to a not-too-small J_{PHE} in Co layer and a moderate J_{SHE} in PtGd layer, there is a strong orbital current due to OHE (J_{OHE}) in Mo layer flowing along the out-of-plane direction, which will be converted into an additional-y-polarized strong spin current when passing through PtGd layer, and will significantly boost τ_y in Co layer. (**d**) The anomalous Hall resistance $\boldsymbol{R_H}$ as a function of an out-of-plane magnetic field $\boldsymbol{H_z}$ for Co(0.8)/Pt(2), Co(0.8)/PtGd(2), and Co(0.8)/PtGd(2)/Mo(2) Hall bar devices, respectively. (**e-f**) Anisotropic magnetoresistance ($\boldsymbol{\Delta\rho_{\text{AMR}}}$) for Co(0.8)/Pt(2), Co(0.8)PtGd(2), and Co(0.8)/PtGd(2)/Mo(2) samples in the x-y plane (**e**) and x-z plane (**f**), where the large scanning field of 1.2 T is applied and the variation of resistances (R_{AMR}) as a function of the rotational angle of the magnetic field direction are measured.

The strongly enhanced AMR may result in notable z-polarized planar Hall current (J_{PHE}) in the Co layer. To show this, we measure the hysteresis loop of the R_{H} versus the out-of-plane magnetic field H_z in the presence of a bias dc current J_x along the x direction. If there was a finite p_z in J_{PHE}, the associated τ_z would cause an abrupt shift of the R_{H}-H_z hysteresis loop when τ_z is sufficiently strong to overcome the intrinsic damping of Co. This approach has been widely used to verify the existence of p_z in SOT devices[20,21,25,37]. We find negligible shift of the loop in the Co(0.8)/Pt(2) sample even for a large J_x, as shown in Fig S3 in supplemental section 3. For Co(0.8)/PtGd(2) sample, we find negligible shift for small J_x, while sizable positive and negative shifts emerge when J_x is large (Fig. 2a), indicating the existence of p_z in Co(0.8)/PtGd(2) sample. We define the shift of the R_{H}-H_z hysteresis loop as $\Delta H_z = H_{center}(J_x^+) - H_{center}(J_x^-)$, where $H_{center}(J_x^\pm) = \frac{[H_r^+(J_x^\pm) + H_r^-(J_x^\pm)]}{2}$ is the centre of the hysteresis loop determined by the difference of positive and negative magnetization-reversal fields $H_r^\pm(J_x^\pm)$, and $J_x^\pm$ are the current density of positive and negative currents. Figure 2b shows the ΔH_z as a function of J_x, where the ΔH_z is negligible when J_x is small and increases linearly when $J_x > 12 \times 10^6$ A/cm^{-2}. This phenomenon cannot occur in conventional SOT devices supporting only p_y, where ΔH_z can only be generated in the presence of an H_x field[20,25,34]. The

effective SOT field $\eta_z = \Delta H_z / J_x$ contributed by p_z is then determined with $H_x = 0$ Oe (Fig. 2b and 2c). Subsequently, using a standard harmonic Hall voltage measurement technique, we evaluate the SOT effective field η_y, as described in Fig. S4d in supplemental section 4. The contribution of p_z from J_{PHE} results in an out-of-plane SOT field efficiency $\eta_z = 0.16 \times 10^{-6}$ Oe A^{-1} cm^2, while the p_y attributed to the spin Hall current (J_{SHE}) yields in-plane SOT field efficiency $\eta_y = 2.01 \times 10^{-6}$ Oe A^{-1} cm^2 (Fig. 2c). Despite these contributions, both η_y and η_z may not be strong enough in the device, as evident from the absence of field-free switching of $\boldsymbol{m}$ in Co/PtGd under an achievable J_x (Fig. 3a). This is in agreement with our previous finding in similar Co/PtGd SOT devices with a thin PtGd layer[28].

We then engineer the spin source to enhance p_y and thus the associated η_y using the recently discovered OHE, which generated a current of electron orbital angular momentum (J_{OHE}) that flows transverse to a longitudinal current[38-41]. OHE can exist in materials with weak SOC, such as Mo, Ru, Ti, and Nb[38,42]. The J_{OHE} can be converted to a spin current when passing through a layer with strong SOC which can be significantly stronger than J_{SHE}, promising for spin-orbit torque generation[43]. We thus insert a Mo layer in the bottom of the PtGd layer in the SOT device, where an out-of-plane J_{OHE} is generated by an in-plane charge current J_x in Mo layer and transformed to a spin current via spin-orbit coupling when flowing through PtGd layer (Fig. 1c). We find the η_y is enhanced by 2 times and 4 times in the presence of the Mo underlayers with the thickness of 2 nm and 4 nm, respectively. Such significant enhancement of η_y clearly proves the efficiency of OHE in the generation of p_y. We also measure the R_H-H_z hysteresis loop shifts for Co(0.8)/PtGd(2)/Mo(a) devices and find that the η_z is slightly increased in the presence of Mo layer. This is consistence with the enhancement of AMR shown in Fig. 1e-1f, proving that the generation of p_z is associated with PHE.
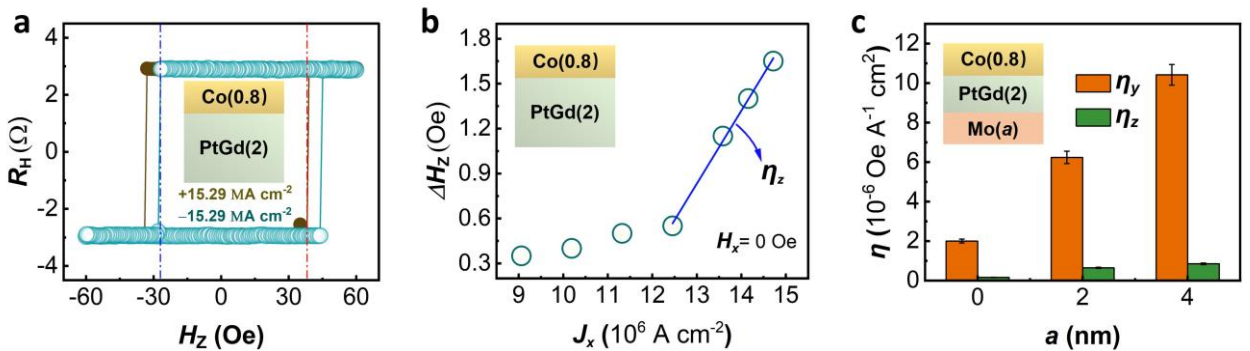
Figure 2: **Finite p_z due to PHE and enhanced p_y due to OHE. (a)** R_{H} vs H_{Z} curves for Co(0.8)/PtGd(2) SOT devices measured by a bias current J_x. **(b)** The R_{H} loop shifts ΔH_{Z} as a function of J_x for Co(0.8)/PtGd(2) SOT devices in the absence of H_x. **(c)** The drive τ_y-associated SOT effective field η_y and τ_z- associated SOT effective field η_z for Co(0.8)/PtGd(2)/Mo(a) SOT devices.

We then prepare Co(0.8)/PtGd(2)/Mo(a) SOT devices with the top Co layer fabricated as pillars to examine the switching behaviour. The thickness of the PtGd layer is fixed to 2 nm to enhance J_{PHE} and facilitate the conversion of J_{OHE} into a spin current J_{SHE}. Figure 3 shows the changes in normalized R_{H} $\left(R_H^{J_x}/R_H^{H_z(S)} \right)$ as a function of an in-plane current J_x applied to these SOT devices. Here, the $R_H^{H_z(S)}$ signifies the saturation magnetization resistance, induced by an out-of-plane magnetic field as shown in Fig. S3 supplemental section 3. In contrast to the flat R_H-J_x curve observed in the absence of Mo ($a = 0$) (Fig. 3a), a hysteretic behaviour and a sign change in R_H-J_x curve emerges when the Mo layer is introduced ($a > 0$) (Figs. 3b and 3c). Notably, we observed about ~100% field-free magnetization switching in the Co pillar for both $a = 2$ nm and 4 nm (Fig. 3b-3c). This observation reflects a substantial y-polarized J_{OHE} and a finite z-polarized J_{PHE} can result in the field-free switching of perpendicular magnetization.
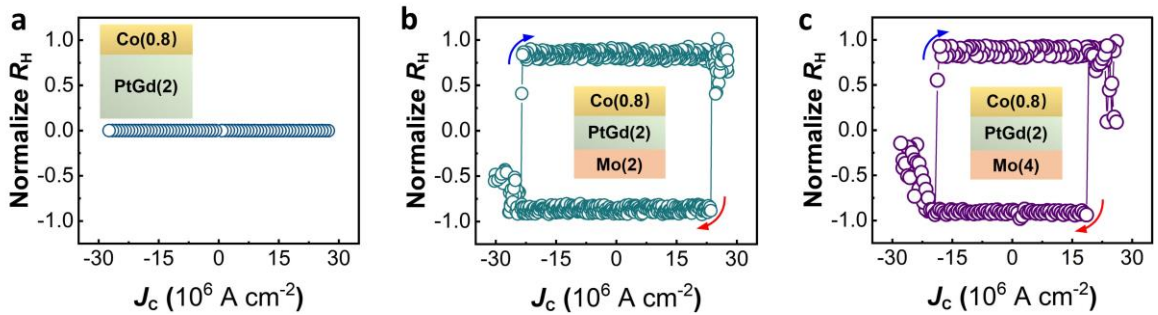

Figure 3: **Field-free current-induced magnetization switching in Co(0.8)/PtGd(2)/Mo(a) SOT pillar-shaped SOT devices. (a-c)** The changes of R_H (normalized) as a function of an in-plane current J_x applied of Co(0.8)/PtGd(2)/Mo(a) SOT devices for $a = 0$ nm **(a)**, $a = 2$ nm **(b)**, and $a = 4$ nm **(c)**. The blue and red arrow shows the SOT switching direction as the switching current sweeps from negative to positive and vice versa.

In conclusion, we have successfully demonstrated the efficient current-induced field-free switching of a perpendicular magnetization in a Co/PtGd/Mo SOT device through the collaborative action of PHE and OHE. The PHE in Co layer is notably enhanced by the Co/PtGd interfacial coupling, resulting in a moderate p_z that contributes to a finite out-of-plane damping-like torque. Simultaneously, the OHE in Mo layer contributes a strong p_y, generating a significant in-plane damping-like torque. With the combined influence of these SOTs, the perpendicular magnetization of Co is efficiently switched without the need for an external magnetic field. Importantly, this approach does not require additional symmetry breaking or particular epitaxy growth for SOT devices, making it particularly attractive for practical applications. Our findings underscore the promising potential of PHE and OHE in magnetic switching and provide a straightforward strategy for the construction of high-performance, and energy-efficient spin-orbitronic devices.

Methods

Thin Film Preparation: The Pt(1.5)/Co(0.8)/Pt$_{0.65}$Gd$_{0.35}$(2)/Mo(a)/Ta(0.5) and the comparative Pt(1.5)/Co(0.8)/Pt(2)/Ta(0.5) (layers from top to down, thicknesses in nanometers) stack structures were grown on thermally oxidized Si/SiO substrate through magnetron sputtering, where a is 0, 2, 3, and 4 nm. The thin films were fabricated at room temperature under a base pressure of better than 3×10^{-8} Torr. The Pt$_{0.65}$Gd$_{0.35}$ alloy films' stoichiometry was achieved by co-sputtering Pt and Gd-targets using direct current (DC) sputtering powers of 30 and 21 W, respectively. Further details of the stoichiometry Pt$_{0.65}$Gd$_{0.35}$ alloy preparation and designs can be found in our prior work[28]. All metal layers were deposited using DC sputtering power without breaking the vacuum chamber. A 1.5 nm Pt layer acts as a capping layer to protect against oxidation of the stack structures. The bottom Mo layer served as a source of orbital Hall current and a 0.5 nm Ta layer is an adhesive layer to promote the PMA of the Co layer. Cr (10 nm)/Au (60 nm) thick electrical contacts were deposited after the second lithography into a pillar-shaped device. No magnetic field was applied during the thin film deposition process.

Fabrication of Devices and Measurements: Before fabrication into the Hall bar device, the stacks are subjected to pre-annealing at 350 $^{\circ}$C for 10 min to persuade PMA. The stacked layers are then patterned into Hall bar devices with a current channel width of 6 μm and a voltage arm width of 3 μm

through photolithography followed by Ar ion milling and a lift-off technique. By applying a 50 μA current along the Hall bar, the anomalous Hall resistances of the devices as a function of the out-of-plane magnetic field are determined. Finally, the Hall bar is further patterned into a pillar-shaped device with a diameter of 3 μm through Ar ion milling to realize field-free SOT switching when the stacks downscaling. Keithley 2602B current source and Keithley 2182 nanovoltmeters were used to measure the current-induced deterministic switching loops by injecting pulsed current along the x-axis. The harmonic Hall voltage was performed using a Stanford Research SR830 DSP lock-in amplifier with a frequency amplitude of 1327 Hz. All measurements of magnetic and electrical properties were conducted at room temperature.

Acknowledgements

Authors Contribution

K.W. conceived and supervised this work. Z. A. B. grew the films, fabricated the devices and carried out the electrical transport measurements. Y. Y. J. and D. F.S. performed the theoretical analysis. Z. A. B., D. F. S., and K. W. analyzed the data and wrote the manuscript. All authors discussed the results and commented on the manuscript.

Competing Interests

The authors declare no competing financial interests.

Data Availability

The data supporting this study findings are available from the corresponding authors upon reasonable request.

References

1. Tsymbal, E.Y., & Žutić, I. (Eds.). (2019). Spintronics Handbook, Second Edition: Spin Transport and Magnetism: Volume Three: Nanoscale Spintronics and Applications (2nd ed.). CRC Press. https://doi.org/10.1201/9780429441189

2. Cao, Y., Rushforth, A., Sheng, Y. et al. Spintronic Synapses: Tuning a Binary Ferromagnet into a Multistate Synapse with Spin–Orbit-Torque-Induced Plasticity. *Adv. Funct. Mater*. **29**, 1970175 (2019).

3. Liu, L., Lee, O. J. et al. Current-induced switching of perpendicularly magnetized magnetic layers using spin torque from the spin hall effect. *Phys. Rev. Lett*. **109**, 096602 (2012).

4. Liu, L. et al. Spin–torque switching with the giant spin Hall effect of tantalum. *Science* **336**, 555 (2012).

5. Miron, I. M. et al. Current-driven spin torque induced by the Rashba effect in a ferromagnetic metal layer. *Nat. Mater*. **9**, 230 (2010).

6. Miron, I. M. et al. Perpendicular switching of a single ferromagnetic layer induced by in-plane current injection. *Nature* **476**, 189 (2011).

7. Fukami, S., Anekawa, T., Zhang, C. & Ohno, H. A spin-orbit torque switching scheme with collinear magnetic easy axis and current configuration. *Nat. Nanotechnol*. **11**, 621 (2016).

8. Fukami, S., et al.. Magnetization switching by spin-orbit torque in an antiferromagnet-ferromagnet bilayer system. *Nat. Mater*. **15**, 535 (2016).

9. Oh, Y. W., Chris Baek, S. H. et al. Field-free switching of perpendicular magnetization through spin-orbit torque in antiferromagnet/ferromagnet/oxide structures. *Nat. Nanotechnol*. **11**, 878 (2016).

10. Lau, Y. C., Betto, D., Rode, K. et al. Spin–orbit torque switching without an external field using interlayer exchange coupling. *Nat. Nanotechnol*. **11**, 758 (2016).

11. Sheng, Y., Edmonds, K. W., Ma, X., et al. Adjustable current-induced magnetization switching utilizing interlayer exchange coupling. *Adv. Electron. Mater*. **4**, 1800224 (2018).

12. Yu, G., Upadhyaya, P., Fan, Y. et al. Switching of perpendicular magnetization by spin–orbit torques in the absence of external magnetic fields. *Nat. Nanotechnol*. **9**, 548 (2014).

13. Cai, K., Yang, M., Ju, H. et al. Electric field control of deterministic current-induced magnetization switching in a hybrid ferromagnetic/ferroelectric structure. *Nat. Mater*. **16**, 712 (2017).

14. You, L., Lee O., Bhowmik, D. et al. Switching of perpendicularly polarized nanomagnets with spin orbit torque without an external magnetic field by engineering a tilted anisotropy. *Proc Natl. Acad. Sci*. **112**, 10310 (2015).

15. Cao, Y., Sheng, Y. et al. Deterministic Magnetization Switching Using Lateral Spin-Orbit Torque. *Adv. Mater*. **32**, 1907929 (2020).

16. Slonczewski, J. C. Current-driven excitation of magnetic multilayers. *J. Magn. Magn. Mater*. **159**, L1 (1996).

17. Lee, K.-S., Lee, S.-W., Min, B.-C. & Lee, K.-J. Threshold current for switching of a perpendicular magnetic layer induced by spin Hall effect. *Appl. Phys. Lett*. **102**, 112410 (2013).

18. Dong-Kyu, L. & Kyung-Jin, L. Spin-orbit torque switching of perpendicular magnetization in ferromagnetic trilayers. *Sci. Rep*. **10**, 1772 (2020).

19. MacNeill, D., Stiehl, G., Guimaraes, M. et al. Control of spin–orbit torques through crystal symmetry in WTe$_2$/ferromagnet bilayers. *Nat. Phys* **13**, 300 (2017).

20. Liu, L., Zhou, C., Shu, X. et al. Symmetry-dependent field-free switching of perpendicular magnetization. *Nat. Nanotechnol*. **16**, 277 (2021).

21. Mahendra, D. C., Shao, D.- F., Hou, V. D.- H. et al. Observation of anti-damping spin-orbit torques generated by in-plane and out-of-plane spin polarizations in MnPd$_3$. *Nat. Mater*. **22**, 591 (2023).

22. Nan, T. et al. Controlling spin current polarization through noncollinear antiferromagnetism. *Nat. Commun*. **11**, 4671 (2020).

23. Chen, X. et al. Observation of the antiferromagnetic spin Hall effect. *Nat. Mater*. **20**, 800 (2021).

24. Bose, A., Schreiber, N.J., Jain, R. et al. Tilted spin current generated by the collinear antiferromagnet ruthenium dioxide. *Nat. Electron.* **5**, 267 (2022).

25. Hu, S., Shao, D.- F., Yang, H. et al. Efficient perpendicular magnetization switching by a magnetic spin Hall effect in a noncollinear antiferromagnet. *Nat. Commun.* **13**, 4447 (2022).

26. Cao, C., Chen, S., Xiao, R.- C. et al. Anomalous anisotropy of spin current in a cubic spin source with noncollinear antiferromagnetism. arXiv:2211.04970 (2022).

27. Ma, Q., Li, Y., Gopman, D. B. et al. Switching a Perpendicular Ferromagnetic Layer by Competing Spin Currents. *Phys. Rev. Lett.* **120**, 117703 (2018).

28. Bekele, Z. A., Liu, X., Cao, Y. & Wang, K. High-Efficiency Spin-Orbit Torque Switching Using a Single Heavy-Metal Alloy with Opposite Spin Hall Angles. *Adv. Electron. Mater.* **7**, 2000793 (2020).

29. Bekele, Z. A. et al. Tuning the High-Efficiency Field-Free Current-Induced Deterministic Switching via Ultrathin PtMo Layer with Mo Content. *Adv. Electron. Mater.* **7**, 2100528 (2021).

30. Lan, X. et al. Field-free spin-orbit devices via heavy-metal alloy with opposite spin Hall angles for in-memory computing, *Appl. Phys. Lett.* **122**, 172402 (2023).

31. Humphries, A. M. et al. Observation of spin-orbit effects with spin rotation symmetry. *Nat. Commun.* **8**, 911 (2017).

32. Amin, V. P., Zemen, J. & Stiles, M. D. Interface-generated spin currents. *Phys. Rev. Lett.* **121**, 136805 (2018).

33. Luo, Z. et al. Spin-orbit torque in a single ferromagnetic layer induced by surface spin rotation. *Phys. Rev. Appl.* **11**, 064021 (2019).

34. Baek, S. C. et al. Spin currents and spin-orbit torques in ferromagnetic trilayers. *Nat. Mater.* **17**, 509 (2018).

35. Safranski, C., Montoya, E. A. & Krivorotov, I. N. Spin-orbit torque driven by a planar Hall current. *Nat. Nanotechnol.* **14**, 27 (2019).

36. Cai, K., Zhu, Z., Lee, J. M. et al. Ultrafast and energy-efficient spin-orbit torque switching in compensated ferrimagnets. *Nat. Electron.* **3**, 37 (2020).

37. Pai, C. F., Mann, M., Tan, A. J. & Beach, G. S. D. Determination of spin torque efficiencies in heterostructures with perpendicular magnetic anisotropy. *Phys. Rev.* B **93**, 144409 (2016).

38. Bernevig, B. A., Hughes, T. L. & Zhang, S.-C. Orbitronics: the intrinsic orbital current in p-doped silicon. *Phys. Rev. Lett.* **95**, 066601 (2005).

39. Kontani, H., Tanaka, T., Hirashima, D., Yamada, K. & Inoue, J. Giant orbital Hall effect in transition metals: origin of large spin and anomalous Hall effects. *Phys. Rev. Lett*. **102**, 016601 (2009).

40. Go, D., Jo, D., Kim, C. & Lee, H.-W. Intrinsic spin and orbital Hall effects from orbital texture. *Phys. Rev. Lett*. **121**, 086602 (2018).

41. Choi, Y. G., Jo, D. et al. Observation of the orbital Hall effect in a light metal Ti. *Nature* **619**, 52 (2023).

42. Ding, S., Ross, A., Go, D. Harnessing Orbital-to-Spin Conversion of Interfacial Orbital Currents for Efficient Spin-Orbit Torques. *Phys. Rev. Lett*. **125**, 177201 (2020).

43. Lee, D., Go, D., Park, H. J. et al. Orbital torque in magnetic bilayers. *Nat. Commun*. **12**, 6710 (2021).